

Strain effects on Li^+ diffusion in solid electrolyte interphases: A molecular dynamics study

Xiang Ji(姬祥) and Junqian Zhang(张俊乾)
Citation: Chin. Phys. B, 2023, 32 (**6**): 066601. DOI: 10.1088/1674-1056/ac9606
Journal homepage: http://cpb.iphy.ac.cn; http://iopscience.iop.org/cpb

What follows is a list of articles you may be interested in

Sintering reaction and microstructure of *M*Al (*M* = Ni, Fe, and Mg) nanoparticles through molecular dynamics simulation

Yuwen Zhang(张宇文), Yonghe Deng(邓永和), Qingfeng Zeng(曾庆丰), Dadong Wen(文大东), Heping Zhao(赵鹤平), Ming Gao(高明), Xiongying Dai(戴雄英), and Anru Wu(吴安如)$
Chin. Phys. B, 2020, 29 (**11**): 116601. DOI: 10.1088/1674-1056/aba2dd

Molecular dynamics simulation of thermal conductivity of silicone rubber

Wenxue Xu(徐文雪), Yanyan Wu(吴雁艳), Yuan Zhu(祝渊), Xin-Gang Liang(梁新刚)
Chin. Phys. B, 2020, 29 (**4**): 046601. DOI: 10.1088/1674-1056/ab7743

Collective diffusion in carbon nanotubes: Crossover between one dimension and three dimensions

Pei-Rong Chen(陈沛荣), Zhi-Cheng Xu(徐志成), Yu Gu(古宇), Wei-Rong Zhong(钟伟荣)
Chin. Phys. B, 2016, 25 (**8**): 086601. DOI: 10.1088/1674-1056/25/8/086601

Diffusion behavior of helium in titanium and the effect of grain boundaries revealed by molecular dynamics simulation

Gui-Jun Cheng(程贵钧), Bao-Qin Fu(付宝勤), Qing Hou(侯氢), Xiao-Song Zhou(周晓松), Jun Wang(汪俊)
Chin. Phys. B, 2016, 25 (**7**): 076602. DOI: 10.1088/1674-1056/25/7/076602

Molecular dynamics simulation of nanoscale surface diffusion of heterogeneous adatoms clusters

Muhammad Imran, Fayyaz Hussain, Muhammad Rashid, Muhammad Ismail, Hafeez Ullah, Yongqing Cai, M Arshad Javid, Ejaz Ahmad, S A Ahmad
Chin. Phys. B, 2016, 25 (**7**): 076601. DOI: 10.1088/1674-1056/25/7/076601

Strain effects on Li^+ diffusion in solid electrolyte interphases: A molecular dynamics study

Xiang Ji(姬祥)[1] and Junqian Zhang(张俊乾)[1,2,†]

[1] *Shanghai Institute of Applied Mathematics and Mechanics, School of Mechanics and Engineering Science, Shanghai University, Shanghai* 200444, *China*

[2] *Shanghai Key Laboratory of Mechanics in Energy Engineering, Shanghai University, Shanghai* 200444, *China*

(Received 9 May 2022; revised manuscript received 20 September 2022; accepted manuscript online 29 September 2022)

Dilithium ethylene dicarbonate (Li_2EDC) and dilithium butylene dicarbonate (Li_2BDC) are the common organic compositions of the solid electrolyte interphase (SEI) layers in rechargeable lithium-ion batteries. The Li^+ diffusion in the amorphous and ordered phases of Li_2EDC and Li_2BDC under various strains has been investigated by using molecular dynamics simulations. It is found that different strains lead to diverse changes in Li^+ diffusivity. The tensile strain makes the Li^+ diffusion coefficients increase in amorphous and ordered Li_2EDC or Li_2BDC, and the compressive strain makes the Li^+ diffusion coefficients decrease in them. The average Li^+ coordination number calculation, ion conductivity calculation and the calculation of the residence autocorrelation function in amorphous and ordered Li_2EDC or Li_2BDC are performed to further analyze the strain effects on Li^+ transport in them. The factors influencing Li^+ diffusion in amorphous and ordered Li_2EDC or Li_2BDC under the strain are discussed.

Keywords: molecular dynamics, alkyl dicarbonate, strain effect, diffusion

PACS: 66.30.–h, 02.70.Ns **DOI:** 10.1088/1674-1056/ac9606

1. Introduction

Rechargeable lithium-ion batteries have been widely used as power sources in portable electronic devices, hybrid electric vehicles and electric vehicles over the last few decades.[1] It is essential to take multiple factors into consideration when designing rechargeable lithium-ion batteries with high performance, long life and high safety, including the reversible capacity of electrode materials, the thermal stability of electrolytes and the properties of solid electrolyte interphase (SEI) layers, etc.[2–5] The SEI layer forms to passivate the electrode surface during lithium-ion battery operation, which prevents further electron transfer between electrode and electrolyte.[6] Hence, the electrons are forced to flow through the external circuit, whereas the lithium ions could transfer through the SEI layers freely to intercalate into the electrodes. Since the SEI layer is where charge transfer occurs, its properties influence the power capability of the lithium-ion battery significantly.[7] Moreover, the SEI layer enhances the chemical stability by preventing further electrolyte reduction decomposition on the electrode surface.[8] The compositions of the SEI layer on different electrodes such as carbon, silicon and lithium metal are different.[9–11] In addition, electrolyte composition also influences SEI composition as well as interfacial impedance.[12,13] In the case of the electrolyte containing ethylene carbonate, the outer part of the SEI layer usually comprises dilithium ethylene dicarbonate (Li_2EDC), and dilithium butylene dicarbonate (Li_2BDC) is also thought to be included in the organic SEI layer of the carbon electrode,[14–16] whereas the inorganic inner layer often contains Li_2CO_3, LiF and Li_2O.[17,18] The SEI layers undergo strains during charge/discharge cycles. Therefore, understanding the strain effects on transport properties of SEI layers is beneficial to the design and improvement of lithium-ion batteries.

A number of experimental studies have been performed to investigate the formation of the SEI layer and its transport properties. Scanning tunneling microscopy (STM) and Fourier transform infrared spectroscopy (FTIR) studies reveal the SEI formation on graphite electrodes and its multistage nature.[19,20] Current-sensing atomic force microscopy (CSAFM) has been employed to exhibit the formation of SEI layer on the cycled $LiNi_{0.8}Co_{0.15}Al_{0.05}O_2$ electrode surface.[21] In addition, the electrochemical impedance spectra (EIS) has been used to quantitatively measure Li-ion diffusivities in SEI layers.[22] Atomistic and *ab initio* simulations have also been carried out to explore the SEI layer formation process and its properties. Leung *et al.* employed *ab initio* molecular dynamics (MD) simulations to study the stability of the SEI layer containing Li_2CO_3 and Li_2EDC on Li metal and Li_xSi surfaces.[23]

Shi *et al.* studied Li^+ diffusion in Li_2CO_3 using first-principles calculations and proposed a two-layer/two-mechanism model of Li^+ transportation through SEI, which included pore diffusion in the outer layer and knock-off diffusion in the inner layer.[24,25] Zhang *et al.* used nonequilibrium MD method to explore lithium transport in inorganic SEI layers.[26] Muralidharan *et al.* adopted a non-polarizable, clas-

†Corresponding author. E-mail: jqzhang2@shu.edu.cn

© 2023 Chinese Physical Society and IOP Publishing Ltd

sical force field to study transport characteristics of Li^+ in the SEI layer composed of Li_2EDC using MD simulation.[27] Borodin *et al.* developed a new polarizable force field, called atomistic polarizable potential for liquids, electrolytes and polymers (APPLE&P), and utilized this force field to investigate the interfacial structure, transport and mechanical properties of the lithium alkyl dicarbonates.[28–30] However, previous studies have not focused on the strain effects on Li^+ diffusion in the SEI layer containing Li_2EDC or Li_2BDC. Understanding how strain effects influence diffusion helps to develop deeper insights into the transport characteristics of Li^+ in the SEI layer. Therefore, it is worthwhile to investigate the Li^+ diffusion in Li_2EDC and Li_2BDC, which has been reported as the components in the organic layer of SEI.[31,32]

In this work, we utilize atomistic MD simulations to explore the transport properties of Li^+ in the amorphous and ordered phases of Li_2EDC and Li_2BDC under various strains. We firstly study amorphous phase, which is studied by many researchers.[33–35] Then we investigate ordered phase because of its existence in the x-ray diffraction pattern.[36] And the results of the investigation of ordered phase can be compared with the previous literatures. The results reveal the relationship between Li^+ diffusivity and strain. Furthermore, the analysis of the strain effects on Li^+ diffusion is given.

2. Computational methods and model

A MD simulation package, WMI-MD, developed by Hooper was adopted to investigate the Li^+ diffusivity in alkyl dicarbonates. The package includes APPLE&P many-body polarization force field, which is suitable for studies of SEI components.[37,38] For our system, an orthogonal simulation box containing 256 Li_2EDC or Li_2BDC molecules was used for the MD simulations. The crystal structure of ordered Li_2EDC and Li_2BDC has not been resolved, but the previous x-ray study shows that ordered Li_2EDC is orthorhombic and has layered structure.[36] Thus, we construct ordered Li_2EDC or Li_2BDC initial configuration by replicating a Li_2EDC or Li_2BDC molecule in the x, y and z directions, which are along three perpendicular edges of the simulation box. The x-, y-axis are parallel to the lithium layers of the ordered system, respectively, and the z-axis is perpendicular to the lithium layers. The amorphous Li_2EDC or Li_2BDC initial configuration was generated from the ordered Li_2EDC or Li_2BDC by performing a 5 ns isothermal-isobaric (NPT) simulation at 900 K. The maximum k vector parameters and the screening parameter for Ewald summation were (8, 8, 8) and 0.19, respectively. The dipole-dipole damping constant parameter was set to 0.2. The amount of reduction applied to the partial charge-induced dipole interaction was 0.2, which is consistent with the parameters used in the study of Borodin *et al.*[28] A multiple time step approach was used, with a 0.5 fs short integration time step for bonded interactions, a 1.5 fs medium time step for nonbonded interactions within 7 Å, and a 3 fs large timestep for nonbonded interactions between 7 Å and 12 Å, calculation of induced dipoles and electrostatic interactions. A Nosé–Hoover thermostat and an Andersen–Hoover barostat were used in this study with the temperature coupling time of 0.1 ps and the pressure coupling time of 100 ps, respectively. Force field parameters are given in the supplementary material. The entire simulations were performed in the NPT and isothermal-isochoric (NVT) ensembles. Firstly, to obtain the equilibrated configuration, the NPT simulations were performed at 450 K and 1 atm. This temperature is adopted because Li^+ shows large displacement on the time scale of a few nanoseconds at relatively high temperature. And ordered phases of alkyl dicarbonates are not stable at temperatures above 500 K.[30] The NPT equilibration simulation runs of amorphous Li_2EDC and Li_2BDC were both 20 ns, and the equilibration simulation runs of ordered Li_2EDC and Li_2BDC were 100 ns and 30 ns, respectively. The snapshots of Li_2EDC and Li_2BDC are shown in Fig. 1. Figures 1(g) and 1(h) are top views of one layer of Li_2EDC and Li_2BDC, respectively. The distribution of Li^+ in such a layer is not homogeneous and represents a percolating 2D network.

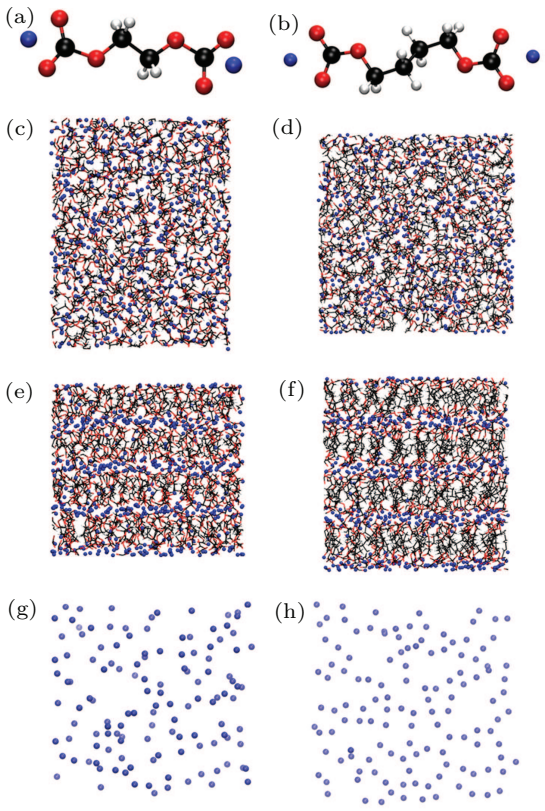


Fig. 1. Snapshots of Li_2EDC and Li_2BDC at 450 K. Black: C; red: O; white: H; blue: Li. (a) The chemical structure of Li_2EDC. (b) The chemical structure of Li_2BDC. (c) Side view of amorphous Li_2EDC. (d) Side view of amorphous Li_2BDC. (e) Side view of ordered Li_2EDC. (f) Side view of ordered Li_2BDC. (g) Top view of one layer of ordered Li_2EDC. (h) Top view of one layer of ordered Li_2BDC.

Next we applied the normal strains between −3% and 3% to equilibrated configuration along different directions. The displacement vector of an atom in the system is determined by the equation

$$x_i - X_i = \sum_{j=1}^{3} X_j \varepsilon_{ij}, \quad (i = 1,2,3 \text{ and } x_1 = x, x_2 = y, x_3 = z), \tag{1}$$

where x_i and X_i are the coordinates of an atom at deformed and initial configuration, and ε_{ij} is the strain tensor. We applied the equal normal strain in x, y and z directions to amorphous Li_2EDC or Li_2BDC, and considered two loading cases for ordered Li_2EDC or Li_2BDC: x–y plane biaxial tensile/compressive strain, i.e., $\varepsilon_{11} = \varepsilon_{22}$, and z direction tensile/compressive strain, i.e., ε_{33}. For both cases, the remaining strain components were set to zero.

Then the MD simulations in the NVT ensemble at 450 K were performed to explore the lithium diffusivity changes under various strains. The Li^+ diffusion coefficient is obtained from the Einstein relation,[39] which can be written as

$$D = \lim_{t\to\infty} \left[\frac{1}{2dt} \left(\frac{1}{N} \sum_{i=1}^{N} \left\langle |\boldsymbol{r}_i(t)|^2 \right\rangle \right) \right], \tag{2}$$

where N is the total number of lithium ions. $\boldsymbol{r}_i(t)$ is the displacement of the ith lithium ion after the simulation time t, and the angle bracket represents the ensemble average. d is the dimension. $d = 3$ and $d = 2$ were adopted for amorphous and ordered phases of alkyl dicarbonates, respectively, since Li^+ diffusion in amorphous phase is three-dimensional, whereas the motion of Li^+ ions is basically confined to a 2D diffusion within the layer of ordered Li_2EDC or Li_2BDC. The NVT simulation runs of all systems were 30 ns, and the 10–30 ns were taken as production runs. The linear regression was used to calculate the Li^+ diffusion coefficients in the production runs of NVT simulations.

3. Results and discussion

Figure 2(a) shows the Li^+ diffusion coefficients in amorphous Li_2EDC and Li_2BDC at 450 K. In both systems, the Li^+ diffusion coefficient increases as the normal strain in x, y and z directions increases in the range of (−3%, 3%). In other words, the tensile strain facilitates the Li^+ diffusion in amorphous Li_2EDC and Li_2BDC, whereas the compressive strain hinders the Li^+ diffusion in them. In addition, lithium ions diffuse faster in amorphous Li_2BDC than in Li_2EDC when no strain is applied, which is in agreement with the result obtained by previous researchers.[30] Figure 2(b) shows the Li^+ diffusion coefficients in ordered Li_2EDC and Li_2BDC at 450 K under different normal strains. Li^+ diffusion coefficient increases as a function of tensile strain, whereas it becomes smaller with increasing the compressive strain. Furthermore, for ordered Li_2EDC and Li_2BDC, Li^+ diffusion coefficient under xy biaxial tensile strain is smaller than the Li^+ diffusion coefficient under tensile strain in z direction.

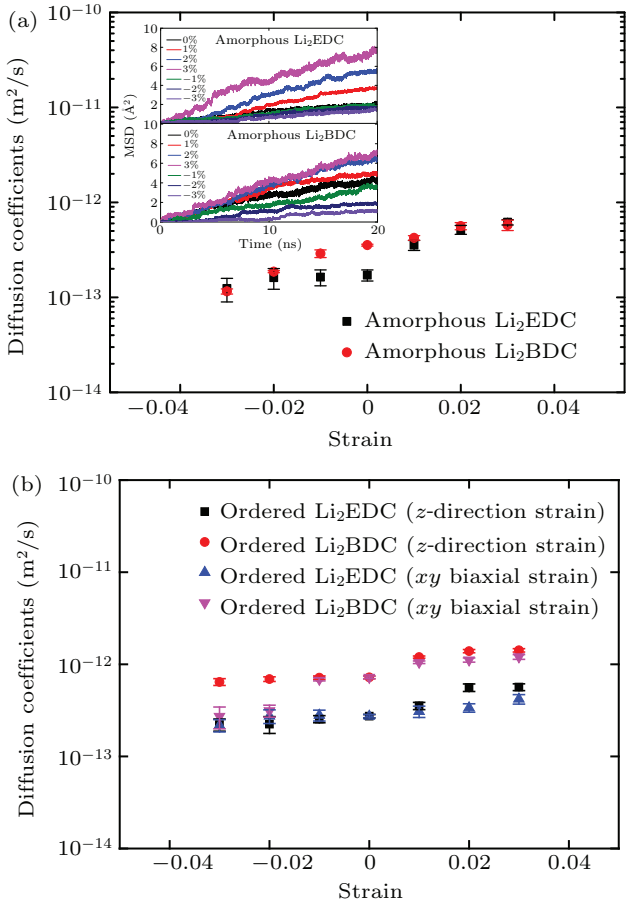


Fig. 2. (a) Li^+ diffusion coefficient varies with normal strain in amorphous Li_2EDC and Li_2BDC at 450 K. Inset: the MSD of Li in amorphous Li_2EDC and Li_2BDC at 450 K under different normal strains (the normal strain in x, y and z direction is equal). (b) Li^+ diffusion coefficient varies with normal strain in different directions in ordered Li_2EDC and Li_2BDC at 450 K. The error bars represent the corresponding standard deviation.

To further analyze the strain effects on Li^+ diffusion in amorphous Li_2EDC and Li_2BDC, we calculate average radial distribution functions $g_{Li-X}(r)$ and average Li^+ coordination numbers (CN), as shown in Fig. 3. $g_{Li-X}(r)$ ($X = O_c$, O_e or Li^+) represents the probability to find atom X at the distance r of Li^+, where X is carbonyl (O_c) oxygen atom, ether (O_e) oxygen atom or lithium ion. Figures 3(a) and 3(b) show $g_{Li-O_c}(r)$, $g_{Li-O_e}(r)$ and $g_{Li-Li}(r)$ in amorphous Li_2EDC and Li_2BDC. Different strains influence little on the average radial distribution functions. The first peaks in the $g_{Li-O_c}(r)$, $g_{Li-O_e}(r)$ and $g_{Li-Li}(r)$ under no strain appear at 2.0 Å, 2.1 Å and 2.9 Å for the amorphous Li_2EDC, and 2.0 Å, 2.1 Å and 2.9 Å for the amorphous Li_2BDC, respectively, which indicate a strong influence of the Li^+ on the O_c, O_e and Li^+. The first minimum in the $g_{Li-O_c}(r)$, $g_{Li-O_e}(r)$ and $g_{Li-Li}(r)$ under no strain appear at 2.8 Å, 2.9 Å and 4.3 Å for the amorphous Li_2EDC, and

2.8 Å, 2.9 Å and 4.2 Å for the amorphous Li_2BDC, respectively, which can be used to define the average Li^+ CN, including CN(O_c), CN(O_e) and CN(Li^+). Figure 3(c) shows the average Li^+ CN for the amorphous Li_2EDC and Li_2BDC under strains. The average Li^+ CN for both amorphous Li_2EDC and Li_2BDC basically decreases with the increase of strain, which reveals that there are less O_c atoms, O_e atoms and lithium ions around the lithium ion when compressive strain is smaller or tensile strain is larger. Therefore, the lithium ion can move easier, resulting a larger diffusion coefficient. The average radial distribution functions for the ordered Li_2EDC and Li_2BDC are similar to the average radial distribution functions for the amorphous Li_2EDC and Li_2BDC at 450 K. Since each Li^+ has more O_c atoms than other atoms in the vicinity ($r < 2.8$ Å), we calculate CN(O_c) to explore the strain effects on Li^+ diffusion in ordered Li_2EDC and Li_2BDC. Figure 3(d) shows the Li^+ CN for the ordered Li_2EDC and Li_2BDC under various strains. With the increase of strain, the Li^+ CN for both ordered Li_2EDC and Li_2BDC decreases. Figure 3(e) shows interlayer spacing (the spacing of Li^+ layer in ordered Li_2EDC and Li_2BDC) under various strains. In both ordered Li_2EDC and Li_2BDC systems, the interlayer spacing under tensile strain in z direction is larger than the interlayer spacing under xy biaxial tensile strain. A lager interlayer spacing allows the Li^+ to consume less energy to move to the adjacent site, resulting a larger diffusion coefficient. Therefore, the Li^+ diffusion coefficient under xy biaxial tensile strain is smaller than Li^+ diffusion coefficient under tensile strain in z direction, which is in consistent with the result in Fig. 2(b). We conclude that Li^+ CN and interlayer spacing are important factors influencing Li^+ diffusion in ordered Li_2EDC and Li_2BDC.

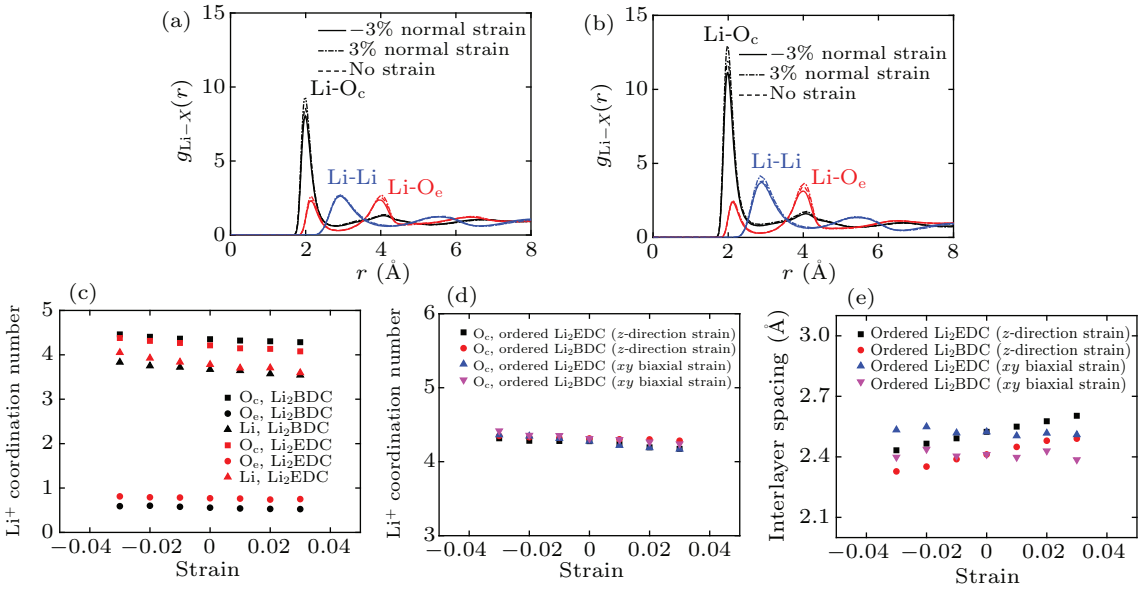


Fig. 3. (a) Average radial distribution functions for the amorphous Li_2EDC at 450 K. (b) Average radial distribution functions for the amorphous Li_2BDC at 450 K. (c) Average Li coordination number for the amorphous Li_2EDC and Li_2BDC at 450 K. (d) Average Li coordination number for the ordered Li_2EDC and Li_2BDC at 450 K. (e) Interlayer spacing as a function of normal strain in different directions at 450 K.

Figures 4(a) and 4(b) show ion conductivity λ in amorphous and ordered Li_2EDC and Li_2BDC at 450 K, which is given by the Einstein relation[40]

$$\lambda = \lim_{t\to\infty} \frac{e^2}{2dtVk_BT} \int_i^n z_i^2 \left\langle |\boldsymbol{r}_i(t)|^2 \right\rangle = \frac{e^2}{Vk_BT} (n_+D_+ + 4n_-D_-), \quad (3)$$

where $\boldsymbol{r}_i(t)$ is the displacement of the ith ion after the simulation time t. d is the dimension. z_i is the charge of the ith ion. e is the electron charge. V, k_B and T are the volume of simulation box, Boltzmann's constant and temperature, respectively. n is the total number of ions. The angle bracket represents the ensemble average. n_+ and n_- are the numbers of cations and anions, respectively. D_+ and D_- are the diffusion coefficients of cations and anions, respectively. In both amorphous Li_2EDC and Li_2BDC systems, the ion conductivity increases with the increase of tensile strain. However, the ion conductivity in amorphous Li_2BDC decreases with the increase of compressive strain. Furthermore, the ion conductivity in amorphous Li_2EDC changes little under compressive strain, which reveals that the motion of ions in amorphous Li_2EDC is retarded less pronounced than in amorphous Li_2BDC under compressive strain. In ordered systems, the ion conductivity in Li_2BDC is larger than in Li_2EDC. Under various strains in ordered systems, the ion conductivity always becomes larger when the tensile strain rises, whereas it goes down when the compressive strain becomes larger.

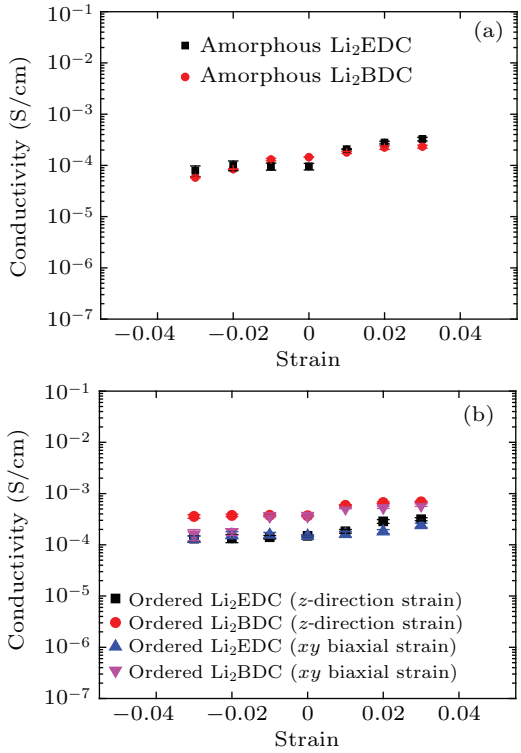


Fig. 4. (a) Ion conductivity varies with normal strain in amorphous Li_2EDC and Li_2BDC at 450 K. (b) Ion conductivity varies with normal strain in ordered Li_2EDC and Li_2BDC at 450 K. The error bars represent the corresponding standard deviation.

The Li^+ residence time can also be used to analyze the strain effects on Li^+ diffusion in amorphous and ordered Li_2EDC or Li_2BDC. A residence autocorrelation function $H(t)H(0)$ is employed to study the Li^+ residence time. t is time, and $H(0)$ is the value of $H(t)$ at $t = 0$. From Fig. 3, we set the first minimum in the $g_{Li-O_c}(r)$, 2.8 Å, as the coordinating shell for Li^+. $H(t) = 1$ when the O_c atom is within the coordinating shell of Li^+. When the O_c atom is out of the coordinating shell of Li^+, $H(t) = 0$. The result of $H(t)H(0)$ gives the probability that the O_c atom within the coordinating shell at the beginning time will still be within the coordinating shell at time t. Figures 5(a) and 5(b) show the Li-O_c residence autocorrelation function in amorphous Li_2EDC and Li_2BDC. The decay of the Li-O_c residence autocorrelation function becomes fast when the tensile strain is applied to both amorphous Li_2EDC and Li_2BDC. However, the decay of the Li-O_c residence autocorrelation function becomes slow under compressive strain in amorphous Li_2BDC, whereas the Li-O_c residence autocorrelation function changes slightly under compressive strain in amorphous Li_2EDC. The results are consistent with the diffusion data in Fig. 2(a), indicating that Li^+ hopping reduces less in amorphous Li_2EDC than in amorphous Li_2BDC under compressive strain. Figures 5(c)–5(f) show the Li-O_c residence autocorrelation function in ordered Li_2EDC and Li_2BDC. The Li-O_c residence autocorrelation function decreases faster with the increase of tensile strain, whereas it decreases slower as compressive strain grows.

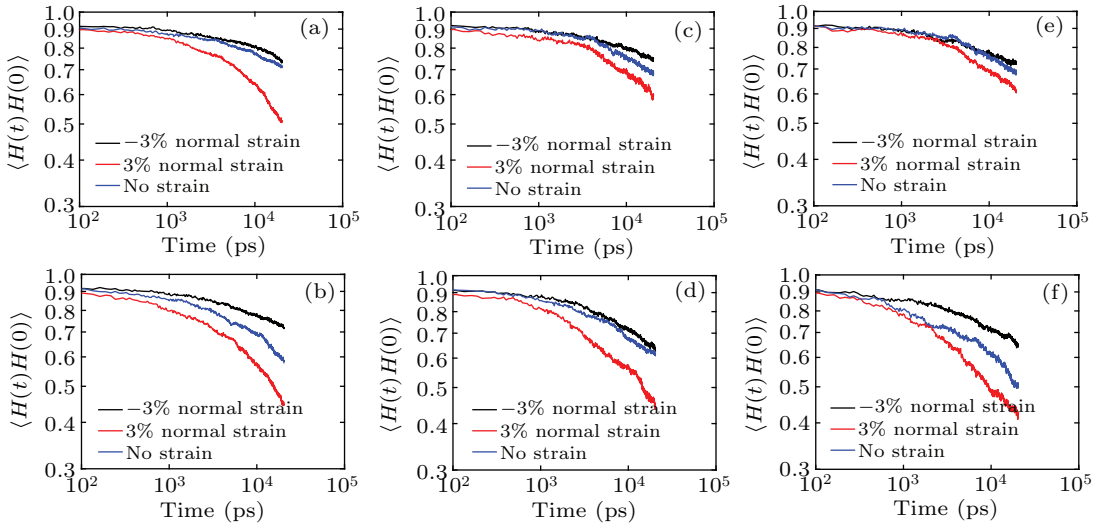


Fig. 5. Li-O_c residence autocorrelation function in (a) amorphous Li_2EDC at 450 K, (b) amorphous Li_2BDC at 450 K, (c) ordered Li_2EDC under the strain in z direction at 450 K, (d) ordered Li_2BDC under the strain in z direction at 450 K, (e) ordered Li_2EDC under xy biaxial strain at 450 K, and (f) ordered Li_2BDC under xy biaxial strain at 450 K.

From Fig. 3(e), we calculate interlayer spacing to study factors influencing Li^+ diffusion in ordered Li_2EDC and Li_2BDC under various strains. The stress effects on Li^+ diffusion in amorphous Li_2EDC and Li_2BDC may be characterized by an activation volume[41,42]

$$\Delta V = \left[RT \frac{\partial \ln (D/D_0)}{\partial \sigma} \right]_T, \tag{4}$$

where D is the Li^+ diffusion coefficients. σ is the hydrostatic stress. D_0 is the constant independent of stress. RT has the usual meaning. Since our study is about the Li^+ diffusion in Li_2EDC and Li_2BDC under the strains, we firstly investigate the relationship of hydrostatic stress and hydrostatic strain, as show in Fig. 6(a). Then we can give the volume of the simulation box as a function of hydrostatic stress, as show in Fig. 6(b). Figure 6(c) shows the relationship between the

diffusion coefficients and the stresses. When tensile stress is applied in amorphous Li_2EDC and Li_2BDC, the diffusion coefficient becomes larger. When compressive stress is applied in amorphous Li_2EDC, the Li^+ diffusion coefficient becomes smaller. Therefore, both activation volumes under tension and compression are positive. Because the diffusion coefficient in amorphous Li_2EDC changes faster under the tension than under the compression, activation volume of amorphous Li_2EDC is larger under the tension than under the compression. However, activation volumes of amorphous Li_2BDC are close under the tension and under the compression because of similar variations of the diffusion coefficients in Li_2BDC under the tension and under the compression. The analysis about the system under stress can also be applied to the system under strain since we have the monotonic increasing relationship of hydrostatic stress and hydrostatic strain.

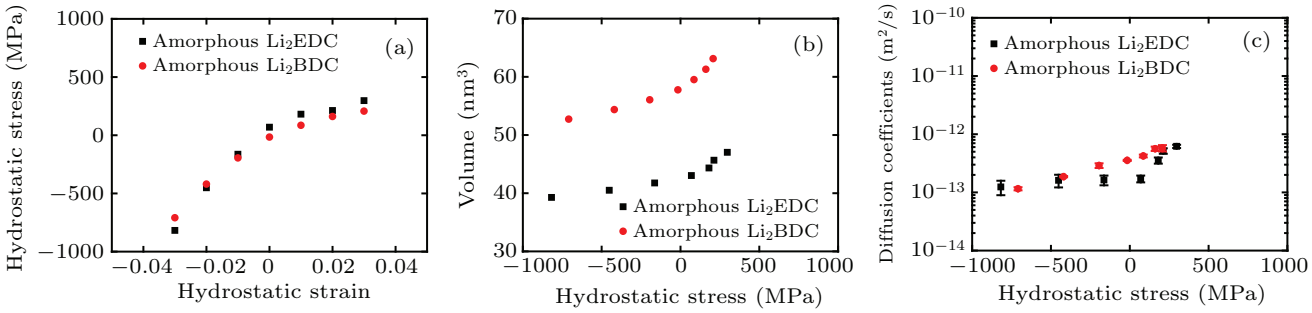


Fig. 6. (a) Hydrostatic stress-strain relationship of amorphous Li_2EDC and Li_2BDC at 450 K. (b) The volume of the simulation box under hydrostatic stress at 450 K. (c) Li^+ diffusion coefficient varies with hydrostatic stress in amorphous Li_2EDC and Li_2BDC at 450 K. The error bars represent the corresponding standard deviation.

4. Conclusion

This work reports the strain effects on Li^+ diffusion in some compositions of the SEI layers, including Li_2EDC and Li_2BDC, using MD simulations. When the tensile strain is applied, the Li^+ diffusion coefficients of the amorphous and ordered Li_2EDC or Li_2BDC increases with the increase of strain. When the compressive strain is applied, the Li^+ diffusion coefficients of the amorphous and ordered Li_2EDC or Li_2BDC decreases with the increase of strain. The average Li^+ CN calculation reveals that there are less O_c atoms, O_e atoms and lithium ions around the lithium ion in amorphous Li_2EDC and Li_2BDC under small compressive strain or large tensile strain, which makes the lithium ion move easier. In ordered Li_2EDC and Li_2BDC, Li^+ CN and interlayer spacing are important factors influencing Li^+ diffusion. The ion conductivity in amorphous Li_2EDC and Li_2BDC increases with the increase of tensile strain. The ion conductivity in amorphous Li_2BDC decreases with the increase of compressive strain, whereas the ion conductivity in amorphous Li_2EDC changes little under compressive strain. In ordered Li_2EDC or Li_2BDC, the ion conductivity increases with the increase of tensile strain, whereas it decreases with the increase of compressive strain. Furthermore, the calculation results of the residence autocorrelation function are consistent with the results of Li^+ diffusion coefficients of the amorphous and ordered Li_2EDC or Li_2BDC. The activation volumes of amorphous Li_2EDC and Li_2BDC under tension and compression are positive. The study results indicate that tensile strain produce positive effects on lithium diffusion as well as ion conductivity in both amorphous and ordered alkyl dicarbonates, which should be considered in the improvement of lithium-ion batteries.

Data availability statement

The data that support the findings of this study are openly available in Science Data Bank at https://doi.org/10.57760/sciencedb.j00113.00069.

Acknowledgements

This work is supported by Shanghai Supercomputer Center.

Project supported by the National Natural Science Foundation of China (Grant No. 11872236).

References

[1] Xu Z, Yang J, Li H, Nuli Y and Wang J 2019 *Mater. Chem. A* **7** 9432
[2] Ji L, Lin Z, Alcoutlabi M and Zhang X 2011 *Energy Environ. Sci.* **4** 2682
[3] Zhang H, Zhao H, Khan M A, Zou W, Xu J, Zhang L and Zhang J 2018 *J. Mater. Chem. A* **6** 20564
[4] Ravdel B, Abraham K M, Gitzendanner R, DiCarlo J, Lucht B and Campion C 2003 *J. Power Sources* **119** 805
[5] Wang A, Kadam S, Li H, Shi S and Qi Y 2018 *npj Comput. Mater.* **4** 1
[6] Peled E and Menkin S 2017 *J. Electrochem. Soc.* **164** A1703
[7] Xu K 2010 *Energies* **3** 135
[8] Xu K 2014 *Chem. Rev.* **114** 11503
[9] Heiskanen S K, Kim J and Lucht B L 2019 *Joule* **3** 2322
[10] Ogumi Z 2010 *Electrochemistry* **78** 319
[11] Yamada Y, Iriyama Y, Abe T and Ogumi Z 2009 *Langmuir* **25** 12766
[12] Wu H, Jia H, Wang C, Zhang J and Xu W 2021 *Adv. Energy Mater.* **11** 2003092
[13] Young B T, Heskett D R, Nguyen C C, Nie M, Woicik J C and Lucht B L 2015 *ACS Appl. Mater. Interfaces* **7** 20004
[14] Hasa I, Haregewoin A M, Zhang L, Tsai W Y, Guo J, Veith G M, Ross P N and Kostecki R 2020 *ACS Appl. Mater. Interfaces* **12** 40879
[15] Wang Y, Nakamura S, Ue M and Balbuena P B 2001 *J. Am. Chem. Soc.* **123** 11708
[16] Aurbach D, Ein-Ely Y and Zaban A 1994 *J. Electrochem. Soc.* **141** L1
[17] Aurbach D, Ein-Eli Y, Markovsky B, Zaban A, Luski S, Carmeli Y and Yamin H 1995 *J. Electrochem. Soc.* **142** 2882
[18] Edström K and Herranen M 2000 *J. Electrochem. Soc.* **147** 3628

[19] Seidl L, Martens S, Ma J, Stimming U and Schneider O 2016 *Nanoscale* **8** 14004
[20] Zhuang G V, Xu K, Jow T R and Ross Jr P N 2004 *Solid State Lett.* **7** A224
[21] Kostecki R, Lei J, McLarnon F, Shim J and Striebel K 2006 *J. Electrochem. Soc.* **153** A669
[22] Cheng X B, Yan C, Peng H J, Huang J Q, Yang S T and Zhang Q 2018 *Energy Storage Mater.* **10** 199
[23] Leung K, Soto F, Hankins K, Balbuena P B and Harrison K L 2016 *J. Phys. Chem. C* **120** 6302
[24] Shi S, Lu P, Liu Z, Qi Y, Hector Jr L G, Li H and Harris S J 2012 *J. Am. Chem. Soc.* **134** 15476
[25] Shi S, Gao J, Liu Y, Zhao Y, Wu Q, Ju W, Ouyang C and Xiao R 2016 *Chin. Phys. B* **25** 018212
[26] Zhang S, Liu Y and Liu H 2020 *Mol. Simul.* **46** 573
[27] Muralidharan A, Chaudhari M I, Pratt L R and Rempe S B 2018 *Sci. Rep.* **8** 1
[28] Borodin O, Zhuang G V, Ross P N and Xu K 2013 *J. Phys. Chem. C* **117** 7433
[29] Borodin O and Bedrov D 2014 *J. Phys. Chem. C* **118** 18362
[30] Bedrov D, Borodin O and Hooper J B 2017 *J. Phys. Chem. C* **121** 16098
[31] Xu K 2004 *Chem. Rev.* **104** 4303
[32] Dudney N J, Hagaman E W, Veith G M and Sacci R L (U.S. Patent) 10 263 246 [2019-04-16]
[33] Chen Z, Soltani A, Chen Y, Zhang Q, Davoodi A, Hosseinpour S, Peukert W and Liu W 2022 *Adv. Energy Mater.* **12** 2200924
[34] von Kolzenberg L, Werres M, Tetzloff J and Horstmann B 2022 *Phys. Chem. Chem. Phys.* **24** 18469
[35] Huang W, Wang J, Braun M R, Zhang Z, Li Y, Boyle D T, McIntyre P C and Cui Y 2019 *Matter* **1** 1232
[36] Xu K, Zhuang G V, Allen J L, Lee U, Zhang S S, Ross Jr P N and Jow T R 2006 *J. Phys. Chem. B* **110** 7708
[37] Borodin O, Smith G D and Fan P 2006 *J. Phys. Chem. B* **110** 22773
[38] Borodin O and Smith G D 2009 *J. Phys. Chem. B* **113** 1763
[39] Kushima A and Yildiz B 2010 *J. Mater. Chem.* **20** 4809
[40] Shen K H and Hall L M 2020 *Macromolecules* **53** 3655
[41] Shewmon P 1963 *Diffusion in solids*, 2nd edn. (New York: McGraw-Hill) pp. 84–86
[42] Södervall U, Friesel M and Lodding A 1990 *J. Chem. Soc. Faraday Trans.* **86** 1293